Clays and Clay Minerals, Vol. 65, No. 3, 155–167, 2017.

EFFECT OF TEMPERATURE ON HALLOYSITE ACID TREATMENT FOR EFFICIENT CHLOROANILINE REMOVAL FROM AQUEOUS SOLUTIONS

Beata Szczepanik[1,2,*], Piotr Słomkiewicz[1,2], Magdalena Garnuszek[1], Paweł Rogala[1], Dariusz Banaś[3,4], Aldona Kubala-Kukuś[3,4], and Ilona Stabrawa[3]

[1] Institute of Chemistry, Jan Kochanowski University, Świętokrzyska 15G, 25-406 Kielce, Poland
[2] The Structural Research Laboratory, Jan Kochanowski University, Świętokrzyska 15G, 25-406 Kielce, Poland
[3] Institute of Physics, Jan Kochanowski University, Świętokrzyska 15, 25-406 Kielce, Poland
[4] Holycross Cancer Center, Artwińskiego 3, 25-734 Kielce, Poland

Abstract—Monochloroanilines and dichloroanilines are important reagents or chemical intermediates in the production of dyes, pharmaceuticals, and agricultural chemicals. These toxic compounds have a large tendency to accumulate in the environment and a low natural biodegradability, so improved methods to remove or sequester them are needed. Halloysite is used as an efficient adsorbent to remove toxic compounds, such as aniline, from aqueous solutions. The purpose of this study was to evaluate whether acid-activated halloysites from the "Dunino" (Poland) strip mine could be effective in the removal of not just aniline but also of its chloro-substituted forms from aqueous solutions. The composition, structure, and morphology of activated halloysites were characterized using the following methods: wavelength dispersive X-ray fluorescence analysis (WDXRF), X-ray diffraction (XRD), X-ray photoelectron spectroscopy (XPS), transmission electron microscopy (TEM), energy dispersive X-ray spectroscopy (EDX), Fourier-transform infrared spectroscopy (FTIR), and N_2 adsorption–desorption analysis. The acid-activated halloysites had an increased ability to remove aniline and chloroanilines from aqueous solutions as the acid activation temperature was increased. This suggests that the acid activation temperature is an important factor that influences the ability of acid activated halloysites to adsorb aromatic amines (anilines) from water. The efficiency of aniline and chloroaniline removal by halloysite activated at 80ºC reached maximum levels, especially for the removal of aniline and 4-chloroaniline. The adsorption isotherm data were best described by the Langmuir adsorption model. The values of the Langmuir adsorption constants were calculated using the inverse liquid chromatography method.

Key Words—Acid Activation, Adsorption, Chloroanilines, Halloysite.

INTRODUCTION

Halloysite is a 1:1 layered mineral with one silica tetrahedral sheet and one alumina octahedral sheet, which is chemically similar to kaolinite, and morphologically it has a specific tubular structure with unit layers separated by a monolayer of water molecules (Joussein *et al*., 2005, Brigatti *et al*., 2006). The tubular nanostructure, chemical stability, high specific surface area and porosity, and large adsorption capacity make halloysite attractive for technological applications (Dong *et al*., 2012, Pasbakhsh *et al*., 2013, Yuan *et al*., 2015). Industrial applications of halloysite are related to the surface properties. Activation of the kaolin group minerals, which is the most common type of acid activation, remarkably improves the specific surface area, porosity, and adsorption capacity (Lenarda *et al*., 2007, Frini-Srasra and Srasra, 2008, Panda *et al*., 2010, Zhang *et al*., 2012, Banaś *et al*., 2013). Acid treatment disaggregates halloysite particles and eliminates impurities, but external and inner layers are partly destroyed (Belver *et al*., 2002, Frini-Srasra and Srasra, 2008; Belkassa *et al*., 2013). Consequently, the adsorption properties of halloysite are influenced by acid activation and the physicochemical properties are changed. Acid activation of halloysite is an effective protocol to improve the adsorption of cationic drug molecules like ofloxacin (Wang *et al*., 2013, 2014a, 2014b) dyes like methylene blue (Zhao and Liu, 2008, Luo *et al*., 2011, Zhang *et al*., 2012) and methyl violet (Liu *et al*., 2011). Halloysite was also used as an efficient adsorbent to remove toxic compounds from effluents (Zhao *et al*., 2013).

Chloroanilines are widely used in the production of polymers, rubber additives, dyes, pharmaceuticals, and pesticides. Chloroanilines are toxic compounds with a large tendency to accumulate in the environment and a low natural biodegradability (Loos *et al*., 2003, Gosetti *et al*., 2010). Adsorption is one of the most effective techniques to remove chloroanilines from aqueous solutions (Laszlo 2005, Angioi *et al*., 2005; Zheng *et al*., 2007; Andini *et al*., 2008; Zampori et al., 2008; Chang *et al*., 2012).

Acid activated halloysite has also been used as an effective adsorbent to remove chloropropham, 3-chloroaniline, 4-chloroaniline, and 3,4-dichloroaniline from aqueous solutions (Szczepanik *et al*., 2014a, 2014b; Matusik, 2016). These recent studies were concerned

* E-mail address of corresponding author:
Beata.Szczepanik@ujk.edu.pl
DOI: 10.1346/CCMN.2017.064056

with the modification of halloysite by sulfuric acid at concentrations up to 60 wt.%, as acid treatment in a strong acidic solution can destroy the crystal structure of halloysite and finally turn it into amorphous silica (White *et al*., 2012). The purpose of the present study was to investigate the influence of temperature at low (25 wt.%) sulfuric acid concentrations on the physico-chemical properties of a raw halloysite that was obtained from the "Dunino" (Poland) strip mine, and to measure the adsorption properties of acid-modified halloysites for the removal of aniline, 2-chloroaniline, 3-chloroaniline, 4-chloroaniline, 2,6-dichloroaniline, 3,5-dichloroaniline, and 2,4,5-trichloroaniline from water.

Firstly, the effect of the method of activation on the structure, morphology, and porosity of acid treated halloysites was systematically investigated using wavelength dispersive X-ray fluorescence (WDXRF), X-ray diffraction (XRD), X-ray photoelectron spectroscopy (XPS), Fourier-transform infrared (FTIR) spectroscopy, transmission electron microscopy (TEM), and Brunauer, Emmett, and Teller (BET, Brunauer *et al*., 1938) specific surface area analyses. Afterwards, the adsorption behavior of the acid-treated halloysite for the removal aniline and the chlorinated derivatives of aniline from water were investigated.

EXPERIMENTAL

Materials

Raw halloysite (DHal) was obtained from the "Dunino" Intermark Company, Legnica, Poland strip mine. Samples of 2-chloroaniline, 3-chloroaniline, 4-chloroaniline, 2,6-dichloroaniline, 3,5-dichloroaniline, and 2,4,5-trichloroaniline (Sigma-Aldrich, Poznan, Poland) were used as received. Aniline (Sigma-Aldrich, Poznan, Poland) was freshly distilled under reduced pressure and stored in a refrigerator prior to use. All the reagents were analytical reagent grade. The starting solution of sulfuric acid had a minimum concentration of 95 wt.% H_2SO_4 (Avantor Performance Materials, Gliwice, Poland).

Acid treatment

The raw halloysite (DHal) was dried, ground in a mill (Fritsch Pulverisette 6 Planetary Mono Ball Mill, Hofstra Group, Ltd. Co, Santa Fe, New Mexico, USA), screened through a 0.2−0.35 mm diameter sieve, and washed with deionized water. In order to activate DHal samples, cleaned 200-g samples were digested in 2 L of 25 wt.% H_2SO_4 in a chemical reactor (IKA Laboratory Equipment, Staufen im Breigau, Germany) at 23, 40, 60, 80, and 100ºC for 4 h. After reaction, the resulting slurries were left to settle for 15 min. The acid-treated halloysites were filtered, washed with deionized water until the pH was >5, dried at 50ºC in a thermal chamber for 24 h, and ground into powder. The final products were labeled AHal23, AHal40, AHal60, AHal80, and AHal100.

Batch adsorption experiments

Batch adsorption experiments were conducted in Erlenmeyer flasks that contained 1 g of adsorbent in 20 mL of ultrapure water prepared using a Millipore (EMD Millipore Corporation, Darmstadt, Germany) water purification system. The flask was agitated in a shaker at 120 rpm for 24 h to wet the adsorbent. Next, 20 mL aliquots of the appropriate aniline solutions were added with solution concentrations of 100 mg/L. The flasks were agitated at 120 rpm and room temperature for 24 h in a rotary shaker to ensure adsorption equilibrium. The solutions were then decanted and filtered to collect the supernatants. The residual aniline and chloroaniline concentrations in the supernatants were determined using a UV-visible method. The following wavelengths were used: 280 nm for aniline, 286 nm for 2-chloroaniline, 287 nm for 3-chloroaniline, 290 nm for 4-chloroaniline, 291 nm for 2,6-dichloroaniline, 254 nm for 3,5-dichloroaniline, and 305 nm for 2,4,5-trichloroaniline. The efficiency of aniline removal (R, %) was calculated using equation 1:

$$R = \left(\frac{C_o - Ce}{C_o}\right) \times 100 \quad (1)$$

where C_o and C_e (mg/L) are, respectively, the initial and equilibrium chloroaniline concentrations.

Characterization methods

The halloysite samples were analyzed using wavelength dispersive X-ray fluorescence (WDXRF) with an AXIOS spectrometer from PANalytical (Almelo, The Netherlands) equipped with a Rh anode X-ray tube with a maximum power of 2.4 kW and with X-ray exit windows placed at 45 degrees just in the front of the sample holder (Szczepanik *et al*., 2015). The X-ray powder diffraction measurements were performed using Bragg−Brentano geometry with an X'Pert Pro MPD diffractometer (PANalytical, Almelo, The Netherlands) equipped with a Cu anode 1.8 kW X-ray tube with a linear exit window. The diffractograms were analyzed quantitatively and qualitatively using the Highscore 3.0e program (Highscore 3.0e manual; PANalytical B.V, Almelo, The Netherlands) using the PDF-2 Release 2009 database of the International Centre for Diffraction Data (Newton Square, Pennsylvania, USA). Quantitative analyses were performed using the Reference Intensity Ratio (RIR) method (Banaś *et al*., 2013) giving an estimated error of ±10% for kaolinite and halloysite and a detection limit of about 1%.

The XPS spectral measurements were performed using a SPECS monoXPS system (SPECS GmbH, Berlin, Germany) equipped with a XR50M Al anode X-ray source, a FOCUS 500 quartz single crystal monochromator, and a PHOIBOS 100 electron analyzer with a one dimensional delay line detector (1D-DLD). The

https://doi.org/10.1346/CCMN.2017.064056 Published online by Cambridge University Press

X-ray tube power was 300 W (15 kV, 20 mA). The spectra were recorded at a take-off angle of 90º with the electron analyzer pass energy equal to 30 eV. Vacuum in the analyzer chamber during the measurements was in the range of $6-8\times10^{-9}$ mbar. For charge compensation, an FG-500 flood gun with electron emission current of I_{em} = 70 mA and an electron energy of U_{em} = 3 eV were used.

The scanning transmission electron microscopy (STEM-HAADF) technique with a high angle annular dark field detector was applied to obtain TEM images of the halloysite samples. The TEM images were recorded using a 200kV FEI TecnaiOsiris transmission electron microscope (FEI Company, Eindhoven, Netherlands) in the Electron Microscopy Laboratory of the Department of Chemistry at Jagiellonian University, Krakow, Poland. The halloysite samples were loaded onto a holey carbon-coated Cu grid (AGAR Scientific). Energy dispersive X-ray spectroscopy (EDX) analyses were carried out in scanning transmission (STEM) mode using SDD-SuperX EDX detectors. The EDX signal was registered in 30 min (10 µs dwell time/pixel). Halloysite samples were prepared as ethanol suspensions by using sonication to disperse the materials. FTIR spectra in the 4000−650 cm^{-1} range were recorded at room temperature using the KBr pellet technique and a Perkin-Elmer Spectrum 400 FTIR/FTNIR spectrometer (Perkin Elmer, Waltham, Massachusetts, USA) at a resolution of 4 cm^{-1}. Before the IR measurements, all samples were dried and powdered by grinding in an agate mortar.

Nitrogen adsorption isotherms were measured at −196ºC using an ASAP 2020 volumetric analyzer manufactured by Micromeritics, Inc. (Norcross, Georgia, USA). All samples were outgassed at 350ºC for 6 h prior to adsorption measurements. The BET (Brunauer-Emmett-Teller, Brunauer *et al*., 1938) specific surface areas, S_{BET}, were calculated from N_2 adsorption isotherms that were measured at 0.05 to 0.2 relative pressures using a cross-sectional area of 0.162 nm^2 per N_2 molecule. The single-point total pore volumes of pores (V_t) were estimated from the volume of N_2 adsorbed at a relative pressure of p/p_0 = 0.99. The volume of mesopores (V_{mez}) was calculated from the difference between the total pore volume and the micropore volume ($V_{mes} = V_t - V_{mik}$). The diameter of halloysite pores (D) was determined based on the relation $D = 4V_t/S_{BET}$ (Paderewski, 1999; Sarbak, 2000).

The aniline and chloroaniline concentrations were measured by the spectrophotometric method using a Shimadzu UV-VIS-NIR UV-3600 (Shimadzu, Kyoto, Japan) spectrophotometer with 1.0 cm quartz cells. The absorbance of solutions was measured at a wavelength that corresponded to the maximum long-wave absorption band of the compounds in water.

Inverse liquid chromatography (ILC) adsorption experiments were conducted using a Thermo Scientific Dionex UltiMate 3000 Series chromatography system (Thermo Fisher Scientific Inc., Waltham, Massachusetts, USA) with a diode array UV detector (DAD). The measurements were controlled by a computer using Chromeleon software (Perkin Elmer, Massachusetts, USA). The peak division method in ILC was applied (Słomkiewicz *et al*., 2015). Halloysite particles were suspended in deionized water and then packed at atmospheric pressure into a 200-mm long column with an inner diameter of 4.0 mm. The HPLC eluent was ultrapure water. Experiments were performed at a temperature of 25±0.1ºC, a 0.1 mL min^{-1} flow rate, injection volume of 50 µL, and a sample concentration of 200 mg/L. The UV absorbance was measured at 280 nm for aniline, 286 nm for 2-chloroaniline and 3-chloroaniline, 290 nm for 4-chloroaniline, 291 nm for 2,6-dichloroaniline, 254 nm for 3,5-dichloroaniline, and 304 nm for 2,4,5-trichloroaniline.

RESULTS AND DISCUSSION

X-ray fluorescence and X-ray diffraction

Elemental analysis measurements for the halloysite samples were performed using the WDXRF technique (Table 1). The chemical compositions of samples AHal100, AHal80, AHal60, AHal40, AHal23, and DHal were as follows: 43−62% O, 2−19% Al, 19−32% Si, 2−12% Fe, 0.7−2% Ti, and <0.1% trace elements. The Al contents in DHal and the acid-activated halloysite prepared at different temperatures decreased in the following order: DHal (18.98%) > AHal23 (18.59%) > AHal40 (18.51%) > AHal60 (12.21%) > AHal80 (6.37%) > AHal100 (2.38%). The Al dissolution is also reflected in the Si/Al mass ratio, which increased from the initial value of 1.01 to 1.03 for AHal23, 1.14 for AHal40, 2.61 for AHal60, 4.28 for AHal80, and 12.94 for AHal100 (values derived from Table 1), clearly indicating that an increased tempera-

Table 1. Elemental composition of the DHal and AHal halloysite samples measured using WDXRF.

Element (wt.%)	DHal	AHal23	AHal40	AHal60	AHal80	AHal100
O	43.91	52.03	48.61	42.57	58.02	61.89
Al	18.98	18.59	18.51	12.21	6.37	2.38
Si	19.19	19.20	21.06	31.92	27.26	30.57
Fe	11.31	9.24	9.41	4.45	3.72	2.71
Ti	0.82	0.83	1.35	1.49	1.86	1.87

https://doi.org/10.1346/CCMN.2017.064056 Published online by Cambridge University Press

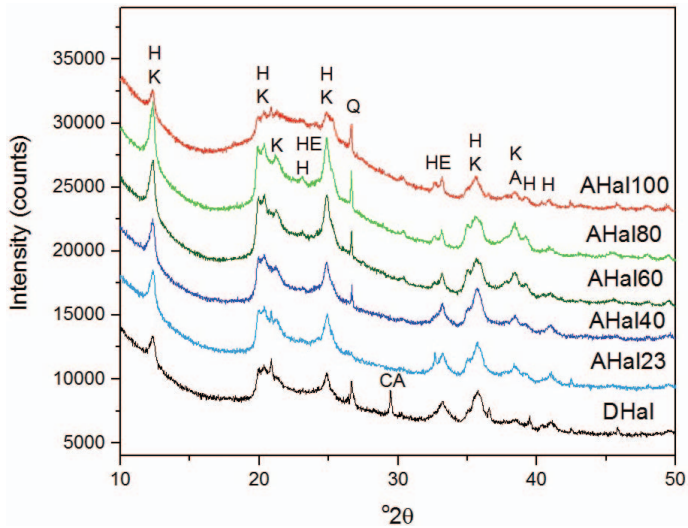

Figure 1. X-ray diffraction patterns of untreated (DHal) halloysite and halloysite samples that were acid activated at temperatures of 23, 40, 60, 80, and 100ºC. Mineral peaks are identified in the diffraction patterns by H = halloysite, K = kaolinite, HE = hematite, CA = calcite, Q = quartz, and A = anatase.

ture during sulfuric acid treatment caused more intense dissolution of the $[AlO_6]_n$ octahedral sheets (Cheng *et al.*, 2011).

The highest content of Fe (11.31%) was observed in the DHal sample and acid activation caused a systematic decrease in the content of Fe in the AHal samples as the activation temperature was increased (Table 1). These results further confirmed that an increase in the temperature during acid digestions of halloysite significantly affected the halloysite composition.

Diffraction patterns of DHal, AHal23, AHal40, AHal60, AHal80, and AHal100 samples (Figures 1) revealed the contents with respect to halloysite, kaolinite, hematite, and calcite minerals. The DHal, AHal23, and AH40 XRPD patterns were very similar to each other except for the different intensities of the hematite peak in the acid treated AHal23 and AHal40 patterns, and the calcite peak in the DHal pattern, which is absent from the acid treated samples. A comparison of XRPD patterns of all samples suggests a systematic increase in the halloysite content in the acid activated samples except for the AHal100 sample. Additionally, the calcite peak was absent in the AHal patterns and the hematite peak intensity was strongly reduced with an increase in the acid activation temperature. Acid activation at 60−100ºC reduced the content of amorphous material in the sample, which was manifested in the diffractograms by an almost two-fold reduction in the background intensity. The intensity of the halloysite/kaolinite peaks in the AHal100 pattern were reduced in comparison to the AHal80 sample, which apparently was caused by structural changes that were confirmed by an increased quartz content (Figure 1, Table 2).

XPS spectra

The XPS spectra were measured for the DHal sample and the acid activated AHal samples. An analysis of the XPS spectra was performed using CasaXPS software (ver. 2.3) which was included with the SPECS XPS system. The following lines in the DHal spectrum were identified: Al 2p, Al 2s, Si 2p, Si 2s, C 1s, Ti 2p, Fe 2p, Fe 2s, O 1s as well as Auger peaks (Fe LMM, O KLL) (Figure 2). The samples were exposed to the atmosphere and a small amount of adventitious carbon with an energy of 282.61 eV was also detected. The presence of Ti 2p, Fe 2p, and Fe 2s lines confirmed that the DHal sample contains

Table 2. Mineral contents (wt.%) in the DHal and AHal halloysite samples (crystalline fraction) measured using XRPD.

Sample	Halloysite + kaolinite	Hematite	Quartz	Anatase
DHal	68	23	3	6
AHal23	76	14	3	7
AHal40	78	14	3	5
AHal60	81	8	3	6
AHal80	84	6	4	4
AHal100	67	5	13	7

https://doi.org/10.1346/CCMN.2017.064056 Published online by Cambridge University Press

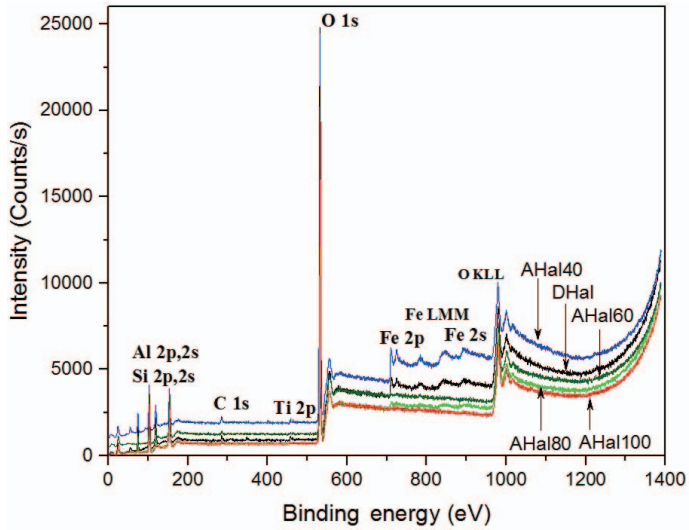

Figure 2. The XPS spectra of the untreated (DHal) halloysite and halloysites acid activated at temperatures of 40, 60, 80, and 100ºC (AHal).

impurities as TiO_2 (anatase) and Fe_2O_3 (hematite) (see Figure 1, DHal diffraction pattern). The Fe can be also assigned to isomorphous substitutions of Fe^{3+} for Al^{3+} in the halloysite octahedral sheet (Ece and Schroeder, 2007). From a comparison of the XPS spectra of the DHal sample to the AHal acid activated halloysite samples (Figure 2), the intensity of lines that originated from Fe and Al were clearly changed. The XPS lines that originated from Fe are nearly absent in samples acid activated at 60−100ºC (AHal60, AHal80, and AHal100). Quantitative surface sensitive results obtained using XPS for the DHal and AHal samples in comparison to the bulk sample results, which were measured with the WDXRF method, showed the differences in the Fe and Ti concentrations. The surface Fe concentrations (Fe 2p XPS) were much lower than the bulk Fe concentrations (XRF) in the DHal (3.81% XPS, 9.61% XRF), AHal40 (6.74% XPS, 9.01% XRF), and AHal60 samples (0.81% XPS, 4.6% XRF). No Fe was observed on the AHal80 and AHal100 sample surfaces, while the bulk Fe contents (XRF) were 2.95% and 2.14%, respectively. Differences in the XPS surface and the XRF bulk Ti contents were especially evident in the AHal80 (0.07% XPS, 1.54% XRF) and AHal100 (0.33% XPS, 1.53% XRF) samples.

Determination of specific surface area and porosity

Adsorption-desorption N_2 isotherms of the raw DHal and acid-treated AHal samples (Figure 3) revealed that the isotherm shapes were very similar and each seemed to be type IV with H3 hysteresis loops according to the IUPAC classification (Balbuena and Gubbins, 1993), which indicates a mesoporous character. This was true for all the halloysite samples. An increase in temperature during acid treatment led to a large increase in both the BET specific surface area (S_{BET}) and total pore volume (V_t) for the AHal samples (AHal80 S_{BET} = 258.6 m^2/g and V_t = 0.37 cm^3/g; AHal100 S_{BET} = 225.5 m^2/g and V_t = 0.41 cm^3/g) in comparison to DHal (DHal S_{BET} = 45.64 m^2/g and V_t = 0.19 cm^3/g) (Table 3). Acid treatment increased the volume of mesopores (V_{mez}) and micropores (V_{mik}), which increased in the following order: DHal < AHal23 < AHal40 < AHal60 < AHal80 < AHal100 (Table 3).

Scanning transmission electron microscopy

The STEM-HAADF images obtained for DHal, AHal80, and AHal100 samples contain tubular, blocky, and platy particles (Figure 4a, 4b). The tube lengths were up to a few hundred nm and were arranged in

Table 3. Specific surface area (S_{BET}), total pore volume (V_t), mesopore volume (V_{mez}), micropore volume (V_{mik}), and pore diameter (D) of the DHal and AHal halloysite samples.

Sample	DHal	AHal23	AHal40	AHal60	AHal80	AHal100
S_{BET} (m^2/g)	45.64	87.65	66.32	201.85	258.60	225.50
V_t (cm^3/g)	0.1925	0.2088	0.2154	0.3043	0.3745	0.4107
V_{mik} (cm^3/g)	0.0019	0.0054	0.0055	0.0565	0.0568	0.0400
V_{mez} (cm^3/g)	0.1906	0.2034	0.2099	0.2475	0.3180	0.3707
D (nm)	16.87	12.56	12.99	6.03	5.79	7.29

https://doi.org/10.1346/CCMN.2017.064056 Published online by Cambridge University Press

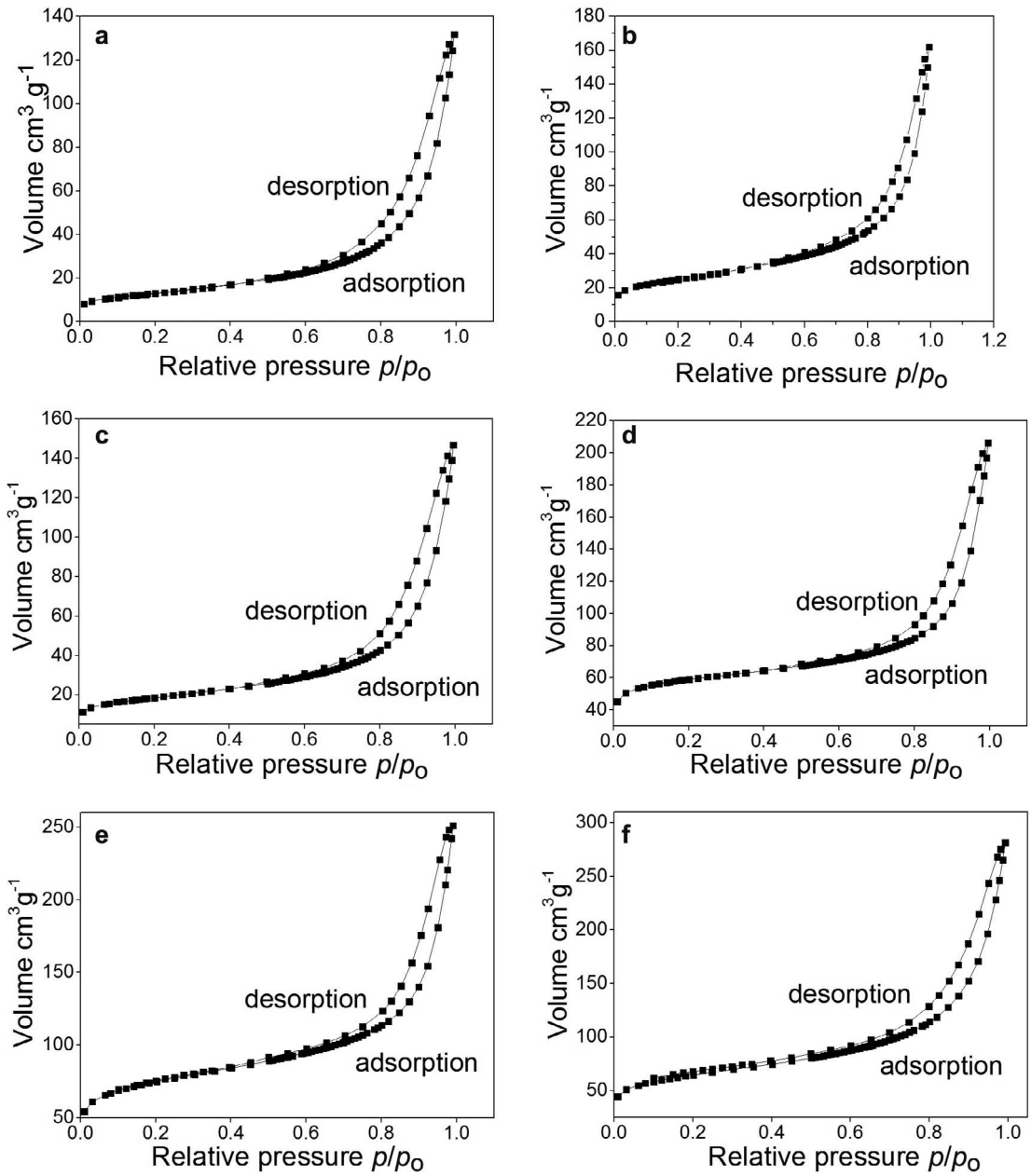

Figure 3. Nitrogen adsorption/desorption isotherms for (a) DHal, (b) AHal23, (c) AHal40, (d) AHal60, (e) AHal80, and (f) AHal100.

various directions. The amorphous material was in the 80ºC and 100ºC acid-treated halloysite samples (Figures 4c–4f). As shown in Figures 4c and 4d, the nanotubes started to peel apart due to 80ºC acid activation. After the 100ºC acid treatment, the surfaces exhibited progressively increased damage, but the tubular character of the particles was preserved (Figure 4e, 4f).

FTIR spectra

The FTIR spectra of the DHal and AHal samples (Figure 5) in the 3800–3550 and 1800–650 cm^{-1} regions exhibited two characteristic bands at 3620 and 3695 cm^{-1}, which were assigned to the stretching vibrations of the inner O–H and the O–H located at the inner-surface of halloysite tubes, respectively (Joussein *et al*., 2005, Cheng *et al*., 2010, 2011). Two weak bands were observed at 3670 and 3655 cm^{-1} for the AHal40 sample. A strong absorption band with well resolved components at 1098, 1037, and 1010 cm^{-1} was attributed to the Si–O–Si stretching band. The bands observed at 938 and 914 cm^{-1} were caused by the O–H deformation of inner-surface hydroxyl groups and O–H

https://doi.org/10.1346/CCMN.2017.064056 Published online by Cambridge University Press

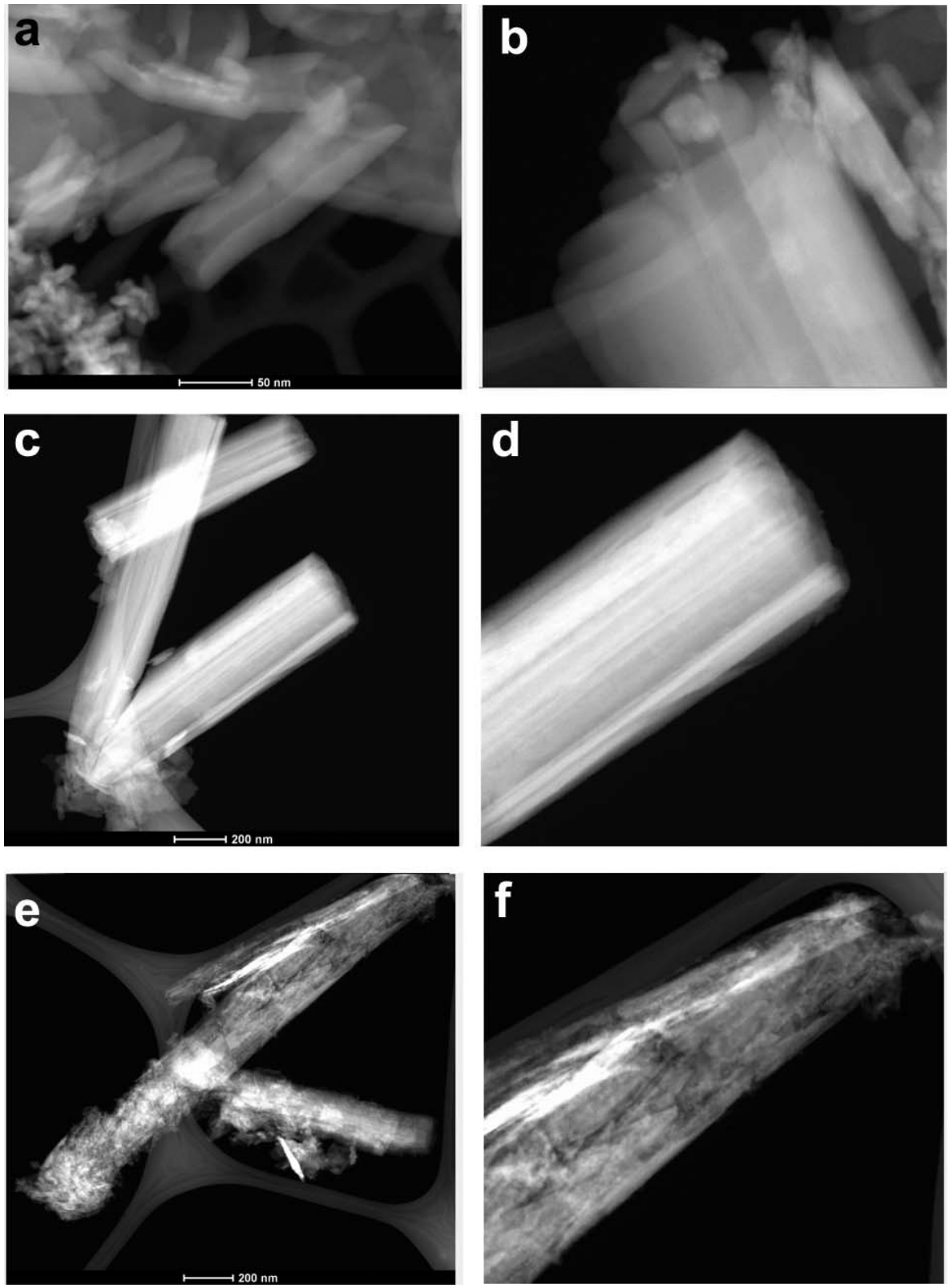

Figure 4. TEM images of (a, b) DHal, (c, d) AHal80, and (e, f) AHal100.

https://doi.org/10.1346/CCMN.2017.064056 Published online by Cambridge University Press

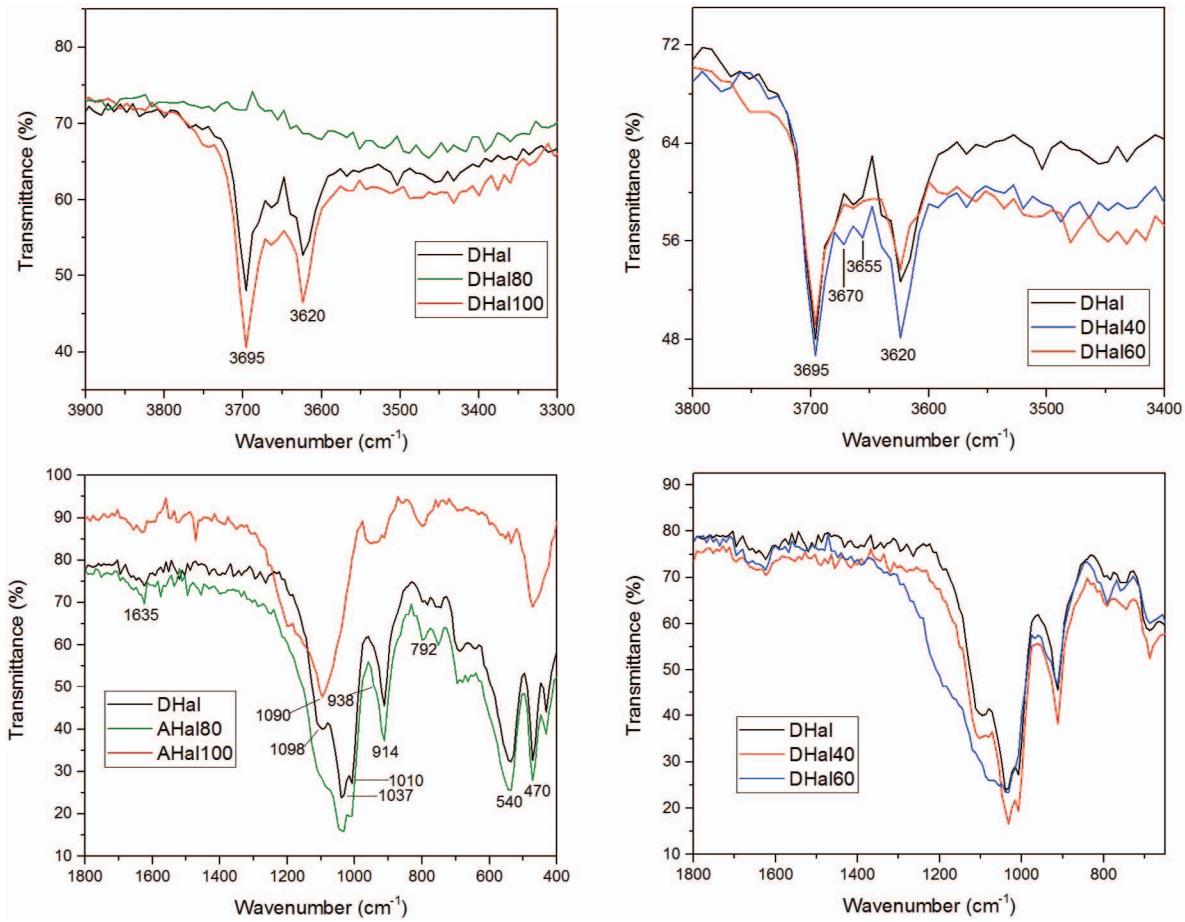

Figure 5. FTIR spectra of DHal and AHal samples in the 3800−3550 cm^{-1} and 1800−650 cm^{-1} regions.

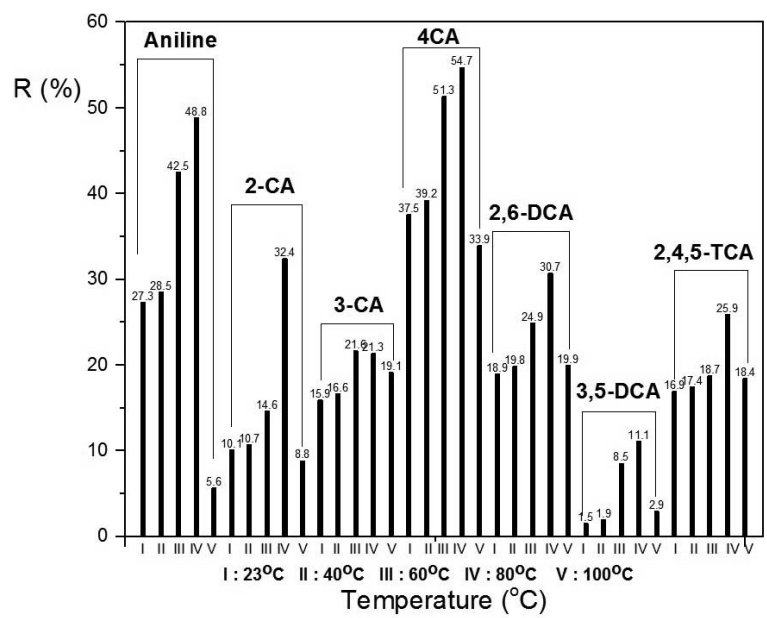

Figure 6. The effect of acid (H_2SO_4) activation temperature (23−100ºC) on aniline, 2-chloroaniline (2-CA), 3-chloroaniline (3-CA), 4-chloroaniline (4-CA), 2,6-dichloroaniline (2,6-DCA), 3,5-dichloroaniline (3,5-DCA), and 2,4,5-trichloroaniline (2,4,5-TCA) removal from aqueous solution by acid activated halloysites.

https://doi.org/10.1346/CCMN.2017.064056 Published online by Cambridge University Press

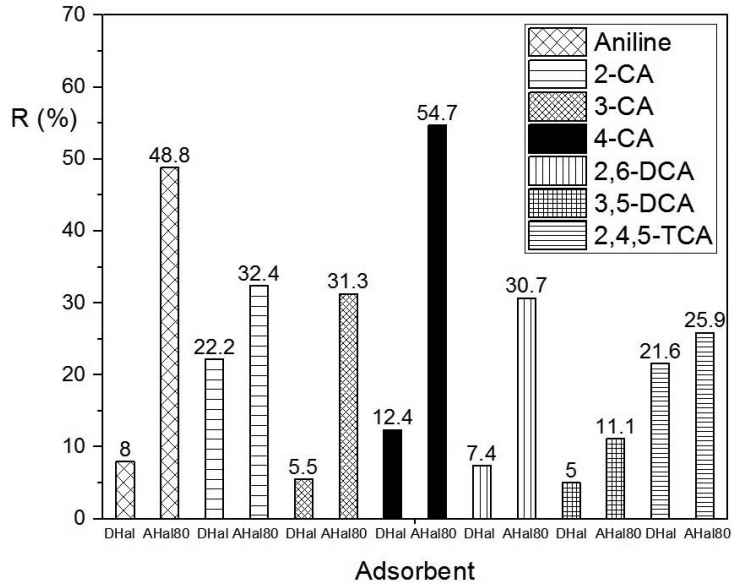

Figure 7. The efficiency of aniline and chloroaniline removal from aqueous solutions by untreated DHal halloysite and AHal80 halloysite (acid activated at 80ºC).

deformation of inner hydroxyl groups, respectively (Joussein *et al*., 2005, Cheng *et al*., 2010, 2011). The band at 540 cm^{-1} was attributed to Si-O-Al bending vibrations and the band at 470 cm^{-1} to Si-O-Si bending vibrations (Madejová and Komadel, 2001, Pentrak *et al*., 2009). Compared to the DHal spectrum, all IR bands in the acid-treated sample (AHal) had increased considerably with relative intensities in the following order: DHal < AHal40 < AHal80. In the case of the AHal100 sample, bands in the 3800−3550 cm^{-1} region disappeared and, in addition, the band at 1035 cm^{-1} broadened and moved to 1090 cm^{-1}.

Batch adsorption experiments

The removal efficiency of all the studied anilines increased with increases in the halloysite acid-activation temperature up to 80ºC (Figure 6). The largest removal efficiency was for halloysite (AHal80) activated at 80ºC with removal efficiencies of 48.8% for aniline, 32.4% for 2-chloroaniline, 21.3% for 3-chloroaniline, 54.7% for 4-chloroaniline, 30.7% for 2,6-dichloroaniline, 11.1% for 3,5-dichloroaniline, and 25.9% for 2,4,5-trichloroaniline. Halloysite acid treatment at 100ºC (AHal100) caused the largest decrease in aniline and 2-chloroaniline removal with 48.8% aniline removal at 80ºC to 5.6% at 100ºC and 32.4% 2-chloroaniline removal at 80ºC to 8.8% at 100ºC. In the case of the other chloroanilines, the decrease in removal was smaller, but noticeable.

Adsorption experiments under the same conditions were also conducted for untreated DHal from the "Dunino" mine for comparison with the acid activated (AHal) halloysites (Figure 7). The DHal sample had weaker adsorptive properties than AHal80 for all the studied anilines with removal efficiencies for aniline, 2-chloroaniline, 3-chloroaniline, 4-chloroaniline, 2,6-dichloroaniline, 3,5-dichloroaniline, and 2,4,5-trichloroaniline of 8.0%, 22.2%, 5.5%, 12.4%, 7.4%, 5%, and 21.6% for DHal and 48.8%, 32.4%, 31.3%, 54.7%, 30.7%, 11.1%, and 25.9% for AHal80, respectively. The AHal80 acid-modified sample proved to be a clearly better adsorbent than DHal.

Determination of adsorption constants using the inverse liquid chromatography method

Previous studies of aniline and 4-chloroaniline adsorption to DHal from aqueous solutions using inverse liquid chromatography employed the method of peak division (Słomkiewicz *et al*., 2015) to allow the calculation of adsorption equilibrium constants using the simplest Langmuir equation (equation 2):

$$a = \frac{K_L c}{1 + K_L c} \quad (2)$$

where a is the amount of solute adsorbed per unit weight of adsorbent at equilibrium (mg/g) (adsorption capacity of adsorbent), K_L is the adsorption equilibrium constant (cm^3/mg), and c is the equilibrium concentration of the adsorbate in the liquid phase (mg/cm^3).

Experimental data from further research on the adsorption of aniline and mono-, di-, and trichloroanilines to raw (DHal) and acid-activated (AHal) halloysites showed that the adsorption mechanism becomes complicated. A few adsorption models were possible, such as (1) adsorption to one active center without dissociation, (2) adsorption to two active centers without dissociation, (3) adsorption to multiple active centers without dissociation, or (4) adsorption to two active centers with dissociation (Thanh *et al*., 1972).

https://doi.org/10.1346/CCMN.2017.064056 Published online by Cambridge University Press

The Langmuir isotherm equation that describes 1/*n*-center adsorption without dissociation (equation 3) was applied to calculate adsorption equilibrium constants for aniline and chloroaniline adsorption to AHal80 based on a best fit of the experimental adsorption data:

$$a = \frac{K_L c^{1/n}}{1 + K_L c^{1/n}} \quad (3)$$

where n is the number of adsorption centers (Figure 8).

The lines in the 2-chloroaniline, 3-chloroaniline, and 4-chloroaniline adsorption isotherms (Figure 8) for AHal80 were fitted to the adsorption data using the Langmuir equation (3). Origin version 2016 MS Windows statistical software was used to determine the isotherm parameters by using the Levenberg-Marquardt least squares method (Origin User's Manual. Microcal Software Inc, Northampton, Massachusetts, USA) to calculate K_L and the correlation coefficient R^2 (Tables 4 and 5). The Langmuir model effectively described the adsorption data with R^2 values from 0.9962 to 0.9999. The K_L values for 2-chloroaniline and 3-chloroaniline adsorption onto AHal80 were comparable and the smallest observed in this study; they were larger for 4-chloroaniline adsorption and largest for aniline adsorption (Table 4). The K_L values were smaller than K_L values for aniline and monochloroanilines and about the same order of magnitude for dichloroanilines and trichloroanilines adsorption to the AHal80 and DHal adsorbents (Table 5).

The calculated number of active centers on the AHal80 adsorbent surfaces were not whole numbers for all of the studied anilines, but were 1.23 for aniline, 1.33 for 2-chloroaniline, 1.26 for 3-chloroaniline, 1.52 for 4-chloroaniline, 1.8 for 2,6-dichloroaniline, 2.1 for 3,5-dichloroaniline, and 1.8 for 2,4,5-trichloroaniline. The aniline and chloroaniline adsorption process to halloysite surfaces probably occurred by several mechanisms at the same time with different numbers of adsorptive centers. As a consequence, the resultant values of the number of active centers is the average value. For the complicated structure of halloysite, exactly identifying active centers is difficult. Adsorption of all the studied anilines was greater by the acid-modified halloysites (AHal) than by the untreated halloysite (DHal), especially for the monochloroanilines. Digesting halloysite with acid modifies the internal aluminol surfaces (-Al-OH) by continuous dissolution of Al^{3+}; chloroaniline molecules may interact with these internal surfaces.

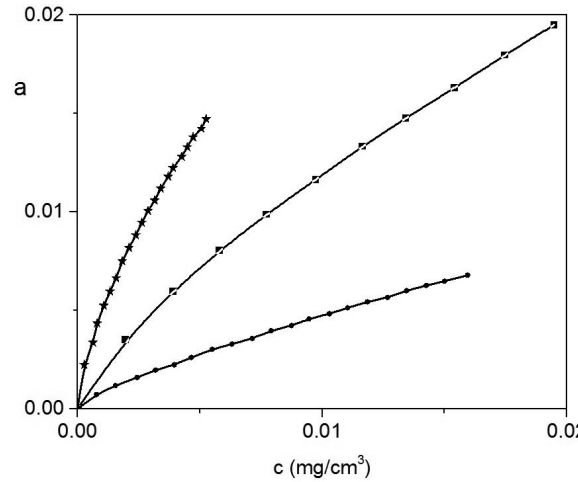

Figure 8. Isotherms for (■) 2-chloroaniline, (●) 3-chloroaniline, and (★) 4-chloroaniline adsorption to AHal80 at 298 K. The curves that connect the data points were fitted to the data using the Langmuir equation by the least-squares method.

CONCLUSIONS

To summarize, the effect of temperature during acid treatment on the structure, morphology, and pore characteristics of the halloysite from "Dunino" mine (Poland) was systematically studied. As revealed by WDXRF chemical analysis, the Si:Al mass ratio systematically decreased as the temperature of acid treatment was increased, from 1:1.1 for AHal40 to 1:12 for AHal100, which suggests that acid treatment dissolved the [AlO_6] octahedral sheets. The XRPD results for acid-activated halloysite samples showed that the hematite content decreased significantly with increasing acid-activation temperature.

The FTIR spectra of the DHal and AHal samples were rather similar in the 1800−650 cm^{-1} region and showed increases in band intensity at acid activation temperatures up to 80ºC. The AHal100 sample showed no increase in band intensities and was the exception for the acid activated halloysites; however, the Si−O−Si in-

Table 4. Langmuir adsorption equilibrium constants, K_L, and correlation coefficients, R^2, for the Langmuir equation fit to adsorption isotherm data for aniline and 2-chloroaniline, 3-chloroaniline, and 4-chloroaniline adsorption to DHal and AHal80 halloysite samples.

	— Aniline —		— 2-CA —		— 3-CA —		— 4-CA —	
Adsorbent	K_L	R^2	K_L	R^2	K_L	R^2	K_L	R^2
DHal	0.583	0.9978	0.220	0.9989	0.181	0.9962	0.321	0.9971
AHal80	0.683	0.9999	0.380	0.9998	0.364	0.9978	0.482	0.9982

https://doi.org/10.1346/CCMN.2017.064056 Published online by Cambridge University Press

Table 5. Langmuir adsorption equilibrium constant, K_L, and correlation coefficient, R^2, for the Langmuir equation fit to adsorption isotherm data for 2,6-dichloroaniline, 3,5-dichloroaniline, and trichloroaniline adsorption to DHal and AHal80 halloysite samples.

Adsorbent	— 2,6-DCA —		— 3,5-DCA —		— 2,4,5-TCA —	
	K_L	R^2	K_L	R^2	K_L	R^2
DHal	0.069	0.9945	0.023	0.9970	0.037	0.9957
AHal80	0.092	0.9981	0.041	0.9986	0.069	0.9968

plane deformation band shifted from 1037 to 1090 cm^{-1}. The bands in the 3800–3550 cm^{-1} range were practically absent in the AHal100 sample, which confirms changes in the mineral structure after acid activation at 100ºC. The FTIR spectra for AHal100 suggest that the acid treatment at 100ºC mostly dissolved the halloysite to leave an amorphous silica residue, which might retain the morphology of the halloysite. The increased intensity of the 792 cm^{-1} band with increased acid treatment temperature and the shift of the Si-O-Si stretching band to 1090 cm^{-1} for the AHal100 sample confirmed increased amounts of amorphous silica (Pentrak *et al.*, 2009).

The TEM images confirmed the nanotubular form of the "Dunino" halloysite samples. The acid treatment at 60–100ºC caused gradual damage to the nanotubes.

Identification of the halloysite 7 Å peak by XRD was ambiguous because the diffraction pattern was almost identical to that of kaolinite (Joussein *et al.*, 2005). Additionally, the FTIR spectra of halloysite samples in the 3800–3550 cm^{-1} region confirmed that kaolinite is present in the "Dunino" halloysite (Madejová and Komadel, 2001). The XRPD, TEM, and FTIR results proved that the halloysite structure was preserved during acid treatment from 23 to 80ºC.

The XPS results suggested that some of the Fe atoms are not bound to the halloysite surface, but are located between the clay particles. Iron was completely removed from halloysite surfaces at activation temperatures >60ºC and this suggests that the halloysite contains Fe built into the bulk phase of halloysite, which did not have contact with H_2SO_4. The isomorphous substitution of Fe^{3+} for Al^{3+} in the octahedral sheet of halloysite crystals is less probable because the AlFeOH band near 3600 cm^{-1} was not observed in the FTIR spectra (Joussein *et al.*, 2005).

The BET surface areas increased 3.9 fold from 66.3 m^2/g for AHal40 to a maximum value of 258.6 m^2/g for AHal80. Total pore volume was mainly represented by mesopores, which were enlarged by increases in acid activation temperature, with total pore volumes that ranged from 0.20 cm^3/g for AHal23 to 0.37 cm^3/g for AHal100.

The AHal adsorbents had an increased ability to remove aniline and chloroanilines from aqueous solutions as the acid activation temperature was increased. The aniline and chloroaniline removal efficiency reached a maximum for halloysite samples activated at 80ºC, especially for aniline and 4-chloroaniline removal. The halloysite acid activated at 80ºC turned out to be an effective low-cost adsorbent for aniline and dichloroanilines. The acid activation temperature played a key role in aniline and chloroaniline adsorption to halloysites activated with sulfuric acid.

The adsorption of aniline and chloroanilines to DHal and AHal adsorbents was described using the Langmuir adsorption model, which suggests that monolayer adsorption occurred in all cases. The values of the adsorption constant calculated using the inverse liquid chromatography method, increased for the AHal adsorbents in the following order: 3-chloroaniline > 2-chloroaniline > 4-chloroaniline > aniline. The adsorption constants for aniline and monochloroaniline adsorption were about an order of magnitude greater than the constants for dichloroaniline and trichloroaniline adsorption, which indicates that interactions of dichloroaniline and trichloroaniline with the halloysite adsorbents were weaker.

ACKNOWLEDGMENTS

Part of this research was carried out using equipment purchased with financial support from the European Regional Development Fund in the framework of the Polish Innovation Economy Operational Program (Contract No. POIG.02.01.00-12-023/08).

REFERENCES

Andini, S., Cioffi, R., Colangelo, F., Montagnaro, F., and Santoro, L. (2008) Adsorption of chlorophenol, chloroaniline and methylene blue on fuel oil fly ash. *Journal of Hazardous Materials*, **157**, 599–604.

Angioi, S., Polati, S., Roa, M., Rinaudo, C., Gianotti, V., and Gennaro, M.C. (2005) Sorption studies of chloroanilines on kaolinite and montmorillonite. *Environmental Pollution*, **134**, 35–43.

Balbuena, P.B. and Gubbins, K.E. (1993) Theoretical interpretation of adsorption behavior of simple fluids in slit pores. *Langmuir*, **9**, 1801–1814.

Banaś, D., Kubala-Kukuś, A., Braziewicz, J., Majewsk,a U., Pajek, M., Wudarczyk-Moćko, J., Czech, K., Garnuszek, M., Słomkiewicz, P. J., and Szczepanik, B. (2013) Study of properties of chemically modified samples of halloysite mineral with X-ray fluorescence and X-ray powder diffraction methods. *Radiation Physics Chemistry*, **93**, 129–134.

Belkassa, K., Bessaha, F., Marouf-Khelifa, K., Batonneau-Generb, I., Comparot, J., and Khelifa, A. (2013)

https://doi.org/10.1346/CCMN.2017.064056 Published online by Cambridge University Press

Physicochemical and adsorptive properties of a heat-treated and acid-leached Algerian halloysite. *Colloids and Surfaces A: Physicochemical and Engineering Aspects*, **421**, 26–33.

Belver, C., Munoz, M.A.B., and Vicente, M.A. (2002) Chemical activation of a kaolinite under acid and alkaline conditions. *Chemistry of Materials*, **14**, 2033–2043.

Brigatti, M.F., Galan, E., Theng, B.K.G., and Lagaly, G. (2006) Structures and mineralogy of clay minerals, in *F. Bergaya, B.K.G. Theng, and G. Lagaly (Eds.) Handbook of Clay Science, Volume 1*. Developments in Clay Science, Elsevier, Amsterdam.

Brunauer, S., Emmett, P.H., and Teller, E. (1938) Adsorption of gases in multimolecular layers. *Journal of the American Chemical Society*, **60**, 309–319.

Chang, Y., Ren, C.-L., Qu, J.-Ch., and Chen, X.-G. (2012). Preparation and characterization of Fe_3O_4/graphene nanocomposite and investigation of its adsorption performance for aniline and p-chloroaniline, *Applied Surface Science*, **261**, 504–509.

Cheng, H., Frost, R.L., Yang, J., Liu, Q., and He, J. (2010) Infrared and infrared emission spectroscopic study of typical Chinese kaolinite and halloysite. *Spectrochimica Acta Part A*, **77**, 1014–1020.

Cheng, H., Liu, Q., Yang, J., Zhang, J., Frost, R. L., and Du, X. (2011) Infrared spectroscopic study of halloysite-potassium acetate intercalation complex. *Journal of Molecular Structure*, **990**, 21–25.

Dong, Y., Liu, Z., and Chen, L. (2012) Removal of Zn(II) from aqueous solution by natural halloysite nanotubes. *Journal of Radioanalytical and Nuclear Chemistry*, **292**, 435–443.

Ece, O. and Schroeder, P. (2007) Hydrothermal alteration of oligocene volcanic rocks and genesis of halloysite-alunite-kaolinite deposits in the Turpla area, Balikesir, Turkey. *Clays and Clay Minerals*, **55**, 18–36.

Frini-Srasra, N. and Srasra, E. (2008) Effect of heating on palygorskite and acid-treated palygorskite properties. *Surface Engineering and Applied Electrochemistry*, **44**, 43–49.

Gosetti, F., Bottaro, M., Gianotti, V., Mazzucco, E., Frascarolo, P., Zampieri, D., Oliveri, C., Viarenga, A., and Gennaro M.C. (2010) Sun light degradation of 4-chloroaniline in waters and its effect on toxicity. A high performance liquid chromatography – Diode array – Tandem mass spectrometry study. *Environmental Pollution*, **158**, 592–598.

Joussein, E., Petit, S., Churchman, G.J., Theng, B.K.G., Righi, D., and Delvaux, B. (2005) Halloysite clay minerals-A review. *Clays and Clay Minerals*, **40**, 383–426.

Laszlo, K. (2005) Adsorption from aqueous phenol and aniline solutions on activated carbons with different surface chemistry. *Colloids and Surfaces A*, **265**, 32–39.

Lenarda, M., Storaro, L., Talon, A., Moretti, E., and Riello, P. (2007) Solid acid catalysts from clays: preparation of mesoporous catalysts by chemical activation of metakaolin under acid conditions. *Journal of Colloid and Interface Science*, **311**, 537–543.

Liu, R.C., Zhang, B., Mei, D.D., Zhang, H.Q. and Liu, J.D. (2011) Adsorption of methyl violet from aqueous solution by halloysite nanotubes. *Desalination*, **268**, 111–116.

Loos, R., Hanke, G., and Eisereich, S.J. (2003) Multicomponent analysis of polar water pollutants using sequential solid-phase extraction followed by LC-ESI-MS. *Journal of Environmental Monitoring*, **5**, 384–394.

Luo, P., Zhang, B., Zhao, Y., Wang. J., Zhang, H., and Liu, J. (2011) Removal of methylene blue from aqueous solutions by adsorption onto chemically activated halloysite nanotubes. *Korean Journal of Chemical Engineering*, **28**, 800–807.

Madejová, J. and Komadel, P. (2001) Baseline studies of the clay minerals society source clays: infrared methods. *Clays and Clay Minerals*, **49**, 410–432.

Matusik, J. (2016) Hallysite for adsorption and pollution remediation. Chapter 23 in: *Developments in Clay Science*, **7**, 606–627.

Paderewski, M. *Adsorption Processes in the Chemical Engineering*. WNT, Warsaw, Poland 1999.

Panda, A.K., Mishra, B.G., Mishra, D.K., and Singh, R.K. (2010) Effects of sulfuric acid treatment on the physico-chemical characteristics of kaolin clay. *Colloids and Surfaces A: Physicochemical and Engineering Aspects*, **363**, 98–104.

Pasbakhsh, P., Churchman, G.J., Jock, G., and Keeling, J.L. (2013) Characterisation of properties of various halloysites relevant to their use as nanotubes and microfibre fillers. *Applied Clay Science*, **74**, 47–57.

Pentrak, M., Madejová, J., and Komadel, P. (2009) Acid and alkali treatment of kaolins. *Clay Minerals* **44**, 511–523.

Sarbak, Z. *Adsorption and Adsorbents. Theory and Application*. WN Poznań, Poland, 2000.

Słomkiewicz, P., Szczepanik, B., and Garnuszek, M. (2015) Determination of adsorption isotherms of aniline and 4-chloroaniline on halloysite adsorbent by inverse liquid chromatography. *Applied Clay Science*, **114**, 221–228.

Szczepanik, B., Słomkiewicz, P., Garnuszek, M., and Czech, K. (2014a) Adsorption of chloroanilines from aqueous solutions on the modified halloysite. *Applied Clay Science*, **101**, 260–264.

Szczepanik, B., Słomkiewicz, P., Garnuszek, M., and Czech, K. (2014b) Adsorption studies of chlorpropham and 3-chloroaniline on chemically activated halloysite. *Journal of Chemistry and Chemical Engineering*, **8**, 626–634.

Szczepanik, B., Słomkiewicz, P., Garnuszek, M., Czech, K., Banaś, D., Kubala-Kukuś, A., and Stabrawa, I. (2015) The effect of chemical modification on the physico-chemical characteristics of halloysite: FTIR, XRF, and XRD studies. *Journal of Molecular Structure*, **1084**, 16–22.

Thanh, L.N., Setinek, K., and Beranek, L. (1972) Kinetics and adsorption on acid catalysts. IV. Kinetics of gas phase dehydration of methanol on sulfonated ion exchanger. *Collection of Czechoslovak Chemical Communications*, **37**, 3878–3884.

Wang, Q., Zhang, J., and Wang A. (2013) Alkali activation of halloysite for adsorption and release of ofloxacin. *Applied Surface Science*, **287**, 54–61.

Wang, Q., Zhang, J., Mu, B., Fan, L., and Wang A. (2014a) Facile preparation of magnetic 2-hydroxypropyltrimethyl ammonium chloride chitosan/Fe_3O_4/halloysite nanotubes microspheres for the controlled release of ofloxacin. *Carbohydrate Polymers*, **102**, 877–883.

Wang, Q., Zhang, J., Zheng, Y., and Wang, A. (2014b) Adsorption and release of ofloxacin from acid- and heat-treated halloysite. *Colloids and Surfaces B: Biointerfaces*, **113**, 51–58.

White, R.D., Bavykin D.V., and Walsh F.C. (2012) The stability of halloysite nanotubes in acidic and alkaline aqueous suspensions. *Nanotechnology*, **23**, 065705.

Yuan, P., Tan, D., and Annabi-Bergaya, F. (2015) Properties and applications of halloysite nanotubes: recent research advances and future prospects. *Applied Clay Science*, **112–113**, 75–93.

Zampori, L., Gallo, Stampino P., Dotelli, G., Botta, D., Natali Sora, I., and Setti, M. (2008) Interlayer expansion of dimethyl ditallowylammonium montmorillonite as a function of 2-chloroaniline adsorption. *Applied Clay Science*, **41** 149–157.

Zhang, A.B., Pan, L., Zhang, H.Y., Liu, S.T., Ye, Y., Xia, M.S., and Chen, X.G. (2012) Effects of acid treatment on the physico-chemical and pore characteristics of halloysite.

Colloids and Surfaces A: Physicochemical and Engineering Aspects, **396**, 182–188.

Zhao, M.F. and Liu P. (2008) Adsorption behavior of methylene blue on halloysite nanotubes. *Microporous and Mesoporous Materials*, **112**, 419–424.

Zhao, Y., Abdullayev, E., Vasiliev. A., and Lvov Y. (2013) Halloysite nanotube clay for efficient water purification. *Journal of Colloid and Interface Science*, **406**, 121–129.

Zheng, K., Pan, B., Zhang, Q., Han, Y., Zhang, W., Pan, B., Xu, Z., Zhang, Q., Du, W., and Zhang, Q. (2007) Enhanced removal of *p*-chloroaniline from aqueous solution by a carboxylated polymeric sorbent. *Journal of Hazardous Materials*, **143**, 462–468.

(*Received 03 January 2017; revised 24 May 2017; Ms. 1156; AE: J. Madejová*)